Estimation of Vector Fields in Unconstrained and Inequality Constrained Variational Problems for Segmentation and Registration

Gozde Unal · Greg Slabaugh

Abstract Vector fields arise in many problems of computer vision, particularly in non-rigid registration. In this paper, we develop coupled partial differential equations (PDEs) to estimate vector fields that define the deformation between objects, and the contour or surface that defines the segmentation of the objects as well. We also explore the utility of inequality constraints applied to variational problems in vision such as estimation of deformation fields in non-rigid registration and tracking. To solve inequality constrained vector field estimation problems, we apply tools from the Kuhn-Tucker theorem in optimization theory. Our technique differs from recently popular joint segmentation and registration algorithms, particularly in its coupled set of PDEs derived from the same set of energy terms for registration and segmentation. We present both the theory and results that demonstrate our approach.

Keywords Variational problems · Equality constraints · Inequality constraints · Kuhn-Tucker theorem · Vector fields · Nonrigid registration · Joint registration and segmentation · Tracking

1 Introduction

Many problems in computer vision and image processing can be posed as variational problems. Examples are im-

G. Unal (✉)
Faculty of Engineering and Natural Sciences, Sabanci University, Tuzla, 34956 Istanbul, Turkey
e-mail: gozdeunal@sabanciuniv.edu

G. Slabaugh
Intelligent Vision and Reasoning, Siemens Corporate Research, Princeton, NJ 08540, USA

age filtering, segmentation, registration, and tracking, which have been extensively solved with variational methods and nonlinear partial differential equations (PDEs). The solutions of such problems generally take the form of images, curves, surfaces, and vector fields, and are sought through an evolution equation defined by a PDE. Usually, an initial estimate of the solution is deformed through a given PDE, which in most cases is derived from optimization (typically minimization) of an energy functional, and occasionally from local heuristics.
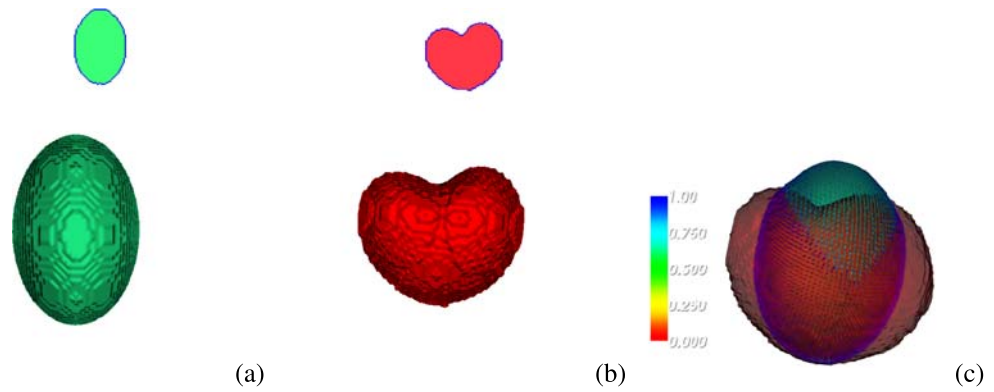
Deformation or displacement fields arise in registration, segmentation, and tracking problems, particularly in the case of multiple image data when a general coordinate transformation is defined between the two image domains. This mapping is usually described through a vector field that transforms one of the image domains to another one. A particular application occurs when a target structure deforms differently in various image volumes, and a joint registration and segmentation approach would be useful if we would like to utilize all the information coming from the multiple images that may be available. In this case, the segmentation and registration processes operate in a coupled way to help each other for an accurate content extraction goal. For instance, in the simplest case, two image volumes consisting of binary regions are shown in Fig. 1 and the goal is to segment the 3D shape from the given multiple image volumes and simultaneously capture the deformation among these volumes as shown in (c).

In many medical imaging applications multiple image volumes in which a structure of interest resides are available. Different modality images of the same region may also be available in some applications. The challenge is then to make use of and relate the existing extra information of a particular organ or structure from several given image volumes. An intuitive idea is to define a vector field that de-

(a)   (b)   (c)

scribes the deformation of the object in different image volumes acquired in different scenarios such as intra-patient (from the same patient at different times and or with different image modalities), and inter-patient image data. Similarly, in dynamic image processing, the velocity of objects are estimated through vector fields that are computed from a sequence of images using temporal and spatial object brightness constraints such as the optical flow equation [18].

As a variational framework is utilized to find solutions to such problems, in some cases, the subset of solutions may be defined by a set of implicit constraints, for example by nonlinear equality or inequality relations. This brings up the question as how to solve variational problems that have constraints. In the case of differential equation constraints, for instance, the solution space has to be confined locally over the domain of the problem, and this turns out to be a nontrivial task.

The popularity and usefulness of variational methods support the efforts for bringing new mathematical tools to the attention of the computer vision community. A general tool that we believe will be useful in variational problems in computer vision and related fields is constrained variational calculus tools for problems such as estimation of a deformation or displacement vector field with inequality constraints.

Motivating examples of inequality constrained problems arise in medical image analysis, for instance the extraction of the left ventricular myocardium from the magnetic resonance (MR) images (see Figs. 11(a) and 12(a)). The object of interest in this case has an annular structure with a change in its thickness during systole and diastole. Normally, the myocardium is segmented with two contours, one inside and one outside, however the problem can be turned into an inequality constrained scenario by utilizing a single contour and its deformation field with certain inequality constraints.

For solving variational problems that have constraints, the method of direct substitution is the most straightforward

procedure, where the constraint equation, if possible, is substituted into the integrand; then the problem is converted into an unconstrained problem. However, this is not possible for the majority of the constrained problems.

Generally, a popular tool that arises is Lagrange multipliers, which always simplify a difficult constrained problem. It should be noted that in a more sophisticated approach, Lagrange multipliers take the form of functions, not the form of constant numbers [21]. When the Lagrange multiplier is a function of the independent variables, this brings an added complication that was not encountered in the types of constraints previously used in the computer vision community.

Constrained problems that are well studied in history of mathematics are: geometrically constrained problems such as the isoperimetric problem, geodesic problems, like the brachistochrone problem, and control theory [11]. Differential forms arise in many constraints, such as the divergence constraint for incompressibility of fluids, or divergence and curl operators in electromagnetism.

1.1 Related Work

As a concrete example to variational problems with and without inequalities, we choose to work with two examples from vision problems: segmentation and registration. Recently, there has been an interest in combining segmentation and registration problems due to a strong interdependence between these two challenging problems of medical image analysis. The joint segmentation and registration idea first introduced by Yezzi et al. [41, 42], estimates rigid registration parameters between two images and a segmentation in a coupled way. An overall energy functional depending on two image regions and registration parameters is minimized resulting in PDEs of both the contour and the registrations through a level set representation [26]. Many of the methods developed in this context used shape prior models in an energy minimization framework [10]. For instance, in [28], a shape model based on a level set representation is constructed and used in an energy to force the evolving interface

to align rigidly with the prior shape. The segmentation energy is separately involved as a boundary and region based energy model. In [37], similarly, a boundary based energy or a Mumford-Shah energy is utilized in conjunction with a distance to a shape prior to which the evolving contour is transformed by a rigid motion. In the same work, the authors also presented an intensity-based PDE which evolves a source image towards a target image, and a coupling PDE to solve for the coordinate transformation from source to the target. This approach however involves a pre-segmentation step, hence is not a joint segmentation and registration approach. Using different criteria for segmentation and rigid registration, an iterative/sequential manner has been carried out in a Bayesian framework in [40]. The same idea of simultaneous segmentation and rigid registration with a prior shape model has been applied to time-varying data for motion estimation and segmentation of moving structures, particularly in cardiac imaging [15]. An active region model based on classical snake nodal constraints with a displacement field defined over the nodes is utilized for again a combined segmentation and motion tracking goal in heart imaging. Almost all of the methods listed above involve only rigid registration as the transformation between two shapes or images.

Wang and Vemuri in [38], also proposed a joint nonrigid registration and segmentation, however, this technique is different from ours in that the registration and segmentation terms in the energy are separate but the coupling between these two operations is only introduced by a third term that checks the distance between the evolved curve and the curve transformed with the deformation field.

Nonetheless, our work is also distantly related to a multitude of tracking techniques, such as [2, 4] that used a region matching through an optical flow constraint, [13, 27] that used a parametric motion model, [43] that matched the distribution of a region with a prior model distribution, or [32] that performed region matching through segmented contours as boundary constraints for registration. On the other hand, it is worth mentioning approaches developed solely for the purpose of nonrigid registration, a popular class of which are variational as well, and solve PDEs for the purpose of nonrigid matching between two image volumes [2, 3, 8]. These techniques are aimed at globally registering image volumes and therefore estimate the deformation field over the whole image. Our technique also solves for a deformation field, however the field is only over the surface. In addition, we also solve for the segmentation in multiple images jointly with the registration.

Analysis and decomposition of vector fields, which are useful functions in many applications, have been studied extensively. For smooth vector fields, Helmholtz-Hodge decomposition [1] provides an intuitive decomposition of a vector field into its components: a rotation-free component, a divergence-free component, and the residuals that are sometimes called the harmonic component. Projection operators were introduced to restore vector field properties such as divergence, curl, and hyperbolic components in [34]. A variational approach was taken in [30] where vector fields on triangulated surfaces were decomposed into a rotation-free, divergence-free and a harmonic component. A multi-scale extension for discrete vector fields was done in [35]. A discrete exterior calculus theory specifically to work with discrete vector fields and operations such as a discrete Hodge decomposition was developed in [14].

Related recent work on constrained variational problems include widely used constraints on vector fields that are referred to as smoothness constraints [2, 8], which only serve the purpose of regularization of the flow. Chefd'hotel et al. utilized matrix constraints such as unit-normness, orthogonality and positive-definiteness in their work that extends and generalizes the variational framework in computer vision from scalar-valued functions to matrix-valued functions [9]. A global constraint on the magnitude of the vector field is utilized in [29] to prevent the vector field from having unnecessarily large amplitudes. In [19], optical flow fields were estimated with a penalty of departure from rigidity, however, without any local inequality constraints like we present here. For myocardium segmentation, image edge and velocity measurements from MR intensity and MR phase contrast images are used to constrain the curve propagation in [39], however this method does not involve a variational constraint approach. An excellent text on image registration, regularization and its numerical solutions can be found in [23].

We also note that equality and inequality constraints using Kuhn-Tucker theorem were utilized in the area of image restoration [5], mainly for setting a nonnegativity constraint for the function which is being restored [20, 25, 31].

1.2 Our Contributions

We present and examine some important mathematical concepts in local equality and inequality constrained variational problems that can be used in problems of computer vision. One contribution of this paper is that we utilize the Kuhn-Tucker theorem to solve for inequality constrained problems in computer vision. Specifically, the solutions to these problems involve locally constrained minimizations with a Lagrange multiplier function that varies with respect to the independent variables. We investigate new avenues with inequality constrained variational formulations which involve spatially varying Lagrange multipliers that may lead to improved solutions for the estimation of vector fields in problems such as segmentation, registration, and tracking.

A second contribution is the generalization of the joint segmentation and registration work of Yezzi et al. [42],

which involved only finite dimensional registrations, but had not foreseen an extension to infinite dimensions. However, a best rigid fit among image volumes will not result in a correct registration in various imaging applications. Therefore, we start with the same joint segmentation and registration idea however improve it to account for more general problems of registration among anatomical structures defined by a deformation field between target regions. The applications are vast such as structures in different MR image sequences (for instance T1 and T2 weighted) or pre and post contrast agent MR images or images of a patient at different time points or images of different patients as well as images of different modalities.

The organization of the paper is as follows. In Sect. 2, we give the fundamentals of the constrained problems in optimization. Section 3 presents the application of constrained calculus of variations problems in computer vision and derives the specific PDEs in Sect. 4. Section 5 presents the experimental results and conclusions.

2 Constrained Problems in the Calculus of Variations

2.1 Fundamentals

Given a bounded region Ω of $\mathbb{R}^n$, we search for a vector function $\boldsymbol{u} : X = \Omega \longrightarrow \mathbb{R}^n$ assigning to each point $\boldsymbol{x}$ in Ω a displacement vector $\boldsymbol{u}(\boldsymbol{x}) \in \mathbb{R}^n$. The set $\mathcal{U}$ on which an extremum problem is defined is called the admissible set. Generally, the set $\mathcal{U}$ is assumed to be a linear subspace of a Hilbert space H, the inner product of which is denoted by $\langle \cdot, \cdot \rangle_H$.

The vector field $\boldsymbol{u} \in Y = C^2(\Omega, \mathbb{R}^n)$ is searched in a set $\mathcal{U}$ of admissible functions such that it minimizes an energy functional $\mathbf{I} : \mathcal{U} \longrightarrow \mathbb{R}$ of the form:

$$F(\boldsymbol{u}) = \int_\Omega f(\boldsymbol{x}, \boldsymbol{u}, D\boldsymbol{u}) d\boldsymbol{x} \tag{1}$$

subject to the functional constraints

$$\Psi(\boldsymbol{x}, \boldsymbol{u}, D\boldsymbol{u}) = \boldsymbol{0}, \tag{2}$$

$$\Phi(\boldsymbol{x}, \boldsymbol{u}, D\boldsymbol{u}) \leq \boldsymbol{0}, \tag{3}$$

where D denotes the Jacobian of $\boldsymbol{u}$.

Definition A function $\boldsymbol{u}$ that satisfies all the functional constraints is said to be *feasible*.

Definition A point at which the *Gateaux differential* of a functional F vanishes, i.e., $\delta F(\boldsymbol{u}^*; \boldsymbol{h}) = 0$ for all the admissible variations $\boldsymbol{h}$, is called a *stationary point*.[1]

From the above definition, it is clear that the *extrema* of a functional F occur at *stationary* points. When the vector space X is normed, a more satisfactory definition of a differential is given by the *Fréchet differential*.

Definition If for each variation $\boldsymbol{h} \in X$ there exists $F'(\boldsymbol{h})$ such that $\lim_{||\boldsymbol{h}|| \to 0} ||F(\boldsymbol{u} + \boldsymbol{h}) - F(\boldsymbol{u}) - F'(\boldsymbol{h})\boldsymbol{h}||/||\boldsymbol{h}|| = 0$, then F is said to be Fréchet differentiable and F' is said to be the *Fréchet differential* of F (see [21] for more details). In the special case, which corresponds to our case, where the transformation F is simply a functional on the space X, F' is called the *gradient* of F, also denoted by ∇F.

2.2 Equality Constrained Problems

Theorem 1 (Lagrange Multiplier) *If the continuously Fréchet differentiable functional F in (1) has a local extremum under the equality constraint (2), $\Psi(\boldsymbol{x}, \boldsymbol{u}, D\boldsymbol{u}) = \boldsymbol{0}$, at the regular point $\boldsymbol{u}^*$, then there exists a function $\mu \in C^2(\Omega, \mathbb{R}^n)$ such that the Lagrangian functional*

$$F(\boldsymbol{x}, \boldsymbol{u}, D\boldsymbol{u}) + \mu(\boldsymbol{x})\Psi(\boldsymbol{x}, \boldsymbol{u}, D\boldsymbol{u}) \tag{4}$$

is stationary at $\boldsymbol{u}^*$, i.e., $F'(\boldsymbol{u}^*) + \mu\Psi'(\boldsymbol{u}^*) = \boldsymbol{0}$.

The intuition with this result is that $F'(\boldsymbol{u}^*)$, the gradient of F, must be orthogonal to the null space of $\Psi'(\boldsymbol{u}^*)$, that is orthogonal to the tangent space.

2.3 Inequality Constrained Problem

A fundamental concept that provides much insight and simplifies the required theoretical development for inequality constrained problems is that of an *active constraint*. An inequality constraint $\Phi(\boldsymbol{x}, \boldsymbol{u}, D\boldsymbol{u})$ is said to be *active* at a feasible solution $\boldsymbol{u}$ if $\Phi(\boldsymbol{u}) = 0$ and *inactive* at $\boldsymbol{u}$ if $\Phi(\boldsymbol{u}) < 0$. By convention, any equality constraint $\Psi(\boldsymbol{u}) = 0$ is *active* at any feasible point. The constraints active at a feasible point $\boldsymbol{u}$ in the set of admissible functions restrict the domain of feasibility in neighborhoods of $\boldsymbol{u}$. On the other hand, inactive constraints, have no influence in neighborhoods of $\boldsymbol{u}$. Inequalities are treated by determining which of them are active at a solution. An active inequality then acts just like an equality except that its associated Lagrange multiplier can never be negative.

Definition A point $\boldsymbol{u}^*$ is a *regular point* if the gradients of the active constraints are linearly independent.

Theorem 2 (Kuhn-Tucker) *Let $\boldsymbol{u}^*$ be a relative minimum point for the problem of minimizing (1) subject to the*

---

[1]If F is a functional on a vector space X, the Gateaux differential of F, if it exists, is $\delta F(\boldsymbol{x}; \boldsymbol{h}) = \frac{d}{dt} F(\boldsymbol{x} + t\boldsymbol{h})|_{t=0}$, and for each fixed

$\boldsymbol{x} \in X$, $\delta F(\boldsymbol{x}; \boldsymbol{h})$ is a functional with respect to the variable $\boldsymbol{h} \in X$. The Gateaux differential generalizes the concept of directional derivative familiar in finite-dimensional space [21].

constraint (3), *and suppose* u^* *is a regular point for the constraints. Then, there is a function* $\lambda \in C^2(\Omega, \mathbb{R}^n)$ *with* $\lambda(x) \geq 0$ *such that the Lagrangian*

$$F(x, u, Du) + \langle \lambda(x), \Phi(x, u, Du) \rangle \qquad (5)$$

is stationary at u^*. *Furthermore,*

$$\langle \lambda(x), \Phi(x, u^*, Du^*) \rangle = 0. \qquad (6)$$

Note that now there are two unknown functions to be estimated: the function $u(x)$ and the Lagrange multiplier $\lambda(x)$ that both vary over the domain Ω. The second necessary condition (6) in the Kuhn-Tucker theorem in addition to the first necessary condition (5) are enough to solve for the two unknowns.

Kuhn-Tucker reformulations for converting the constrained problems into unconstrained problems are presented in [6, 16]. In addition, an interesting approach is presented in [17] with new numerical solutions to the integral forms of the Euler-Lagrange equations for constrained problems.

Types of Constraints There are multitude of different constraint functions that can be used in constraining a cost functional. There is no clear classification, but the ones we came across are as follows. Local constraints are also called as "algebraic constraints", i.e. $G(x) = 0$ (in mechanics called "holonomic constraints"). There are "differential equation constraints", which we are interested in, $G(x, u, u') = 0$ are local constraints (in mechanics called "non-holonomic constraints"), and result in a Lagrange multiplier, which is a function of the independent variable, like $\lambda(x)$. On the other hand, the "integral constraints" are global constraints, and result in a single constant Lagrange multiplier number λ.

3 Applications

For specific applications of the above theorems, we will show in the framework of the calculus of variations, specific examples that will be useful in various computer vision scenarios. Because the case of equality constraints is a special case for the inequality constraints, we opted to study inequality constrained problems as applied to problems in segmentation, registration, and tracking.

In the framework of calculus of variations with inequality constraints, our problem is to minimize

$$F(u) = \int_{\Omega} f(x, u, Du) dx \qquad (7)$$

subject to $\quad \Phi(x, u, Du) \leq 0 \qquad (8)$

where both f and Φ are real-valued, and are assumed to have continuous partial derivatives of second order. Directly

from the Kuhn-Tucker Theorem 2, we will derive the necessary conditions for the minimizer. The first necessary condition is obtained as follows:

$$\frac{\partial}{\partial t}\{F(x, u + th, D(u + th)) + \langle \lambda(x), \Phi(x, u + th, D(u + th)) \rangle\}|_{t=0} = 0. \qquad (9)$$

Hence, we look for the differential of the new Lagrangian $J = F + \langle \lambda, \Phi \rangle$:

$$\delta J(u; h)$$
$$= \frac{\partial}{\partial t} \int_{\Omega} f(x, u + th, D(u + th)) dx$$
$$+ \frac{\partial}{\partial t} \int_{\Omega} \Phi(x, u + th, D(u + th)) \lambda(x) dx. \qquad (10)$$

By the chain rule, the differential $\delta J(u; h)$ can be obtained as the first necessary condition when equated to zero:

$$\delta J(u; h) = \int_{\Omega} f_u(x, u, Du) h \, dx$$
$$+ \int_{\Omega} f_{Du}(x, u, Du) Dh \, dx$$
$$+ \int_{\Omega} \Phi_u(x, u, Du) h \lambda(x) \, dx$$
$$+ \int_{\Omega} \Phi_{Du}(x, u, Du) Dh \lambda(x) \, dx. \qquad (11)$$

In this equation, u and Du in the subscripts denote the variation of a functional, e.g. of f and Φ with respect to the functions u and Du. Integrating (11) by parts,

$$\int_{\Omega} \left\{ \int_{\Omega} f_u dx - f_{Du} + \int_{\Omega} \Phi_u d\lambda(x) - \Phi_{Du} d\lambda \right\} Dh \, dx = 0 \qquad (12)$$

for all variations h vanishing at the boundary of the bounded domain Ω. The resulting Euler-Lagrange equation in its integral form is thus

$$\int_{\Omega} f_u dx - f_{Du} + \int_{\Omega} \Phi_u d\lambda(x) - \Phi_{Du} d\lambda = 0. \qquad (13)$$

In its more familiar differential form, the Euler-Lagrange equations reduce to:

$$f_u - \nabla f_{Du} + \Phi_u \lambda(x) - \Phi_{Du} \nabla \lambda(x) = 0. \qquad (14)$$

The second necessary condition from the Kuhn-Tucker theorem (6) is given by the equation:

$$\int_{\Omega} \Phi(x, u, Du) \lambda(x) dx = 0, \qquad (15)$$

where $\lambda(x)$ is continuous and of bounded variation over the domain Ω. The intuition behind this condition comes from

the idea of active and inactive constraints. The Lagrange multiplier function $\lambda(\boldsymbol{x})$ becomes active over the domain Ω only when the equality is satisfied, and vanishes when the strict inequality is satisfied, that is:

$$\Phi(\boldsymbol{x}, \boldsymbol{u}, D\boldsymbol{u}) < \boldsymbol{0} \text{ (inactive constraint)} \rightarrow \lambda(\boldsymbol{x}) = \boldsymbol{0}, \quad (16)$$

$$\Phi(\boldsymbol{x}, \boldsymbol{u}, D\boldsymbol{u}) = \boldsymbol{0} \text{ (active constraint)} \rightarrow \lambda(\boldsymbol{x}) > \boldsymbol{0}. \quad (17)$$

3.1 Algorithm

We summarize the proposed algorithm for clarity. The coupled equations consisting of (14) with the auxiliary equation (15) forms a complete set of equations to solve for the unknowns $\boldsymbol{u}(\boldsymbol{x})$ and $\lambda(\boldsymbol{x})$ over the domain Ω. The specifics of the cost functional f will be given in the next subsections. To set up the iterations for the PDEs, an artificial time variable t is introduced, and the PDE from (14) to be solved is

$$\frac{\partial \boldsymbol{u}(\boldsymbol{x}, t)}{\partial t} = -f_{\boldsymbol{u}} + \nabla f_{D\boldsymbol{u}} - \Phi_{\boldsymbol{u}}\lambda(\boldsymbol{x}, t) + \Phi_{D\boldsymbol{u}}\nabla\lambda(\boldsymbol{x}, t). \quad (18)$$

Using the time as a new variable, the auxiliary equation in (15) becomes

$$\int_{\Omega} \Phi(\boldsymbol{x}, \boldsymbol{u}(\boldsymbol{x}, t), D\boldsymbol{u}(\boldsymbol{x}, t))\lambda(\boldsymbol{x}, t)d\boldsymbol{x} = \boldsymbol{0}. \quad (19)$$

Without the specifics of the functionals f and Φ, the general algorithm proceeds as follows:

(1) At time $t_0 = 0$, start with a fixed initial value $\boldsymbol{u}^0 = \boldsymbol{u}(t_0)$ that satisfies $\Phi(\boldsymbol{x}, \boldsymbol{u}(\boldsymbol{x}, t_0), D\boldsymbol{u}(\boldsymbol{x}, t_0)) < \boldsymbol{0}$. Then initial value of $\lambda(\boldsymbol{x}, t)$ is automatically fixed $\lambda^0 = \lambda(\boldsymbol{x}, t_0) = 0$.
(2) At time step, $t_k = k\Delta t$, solve for $\boldsymbol{u}^k = \boldsymbol{u}(\boldsymbol{x}, t_k)$ from (18) using $\boldsymbol{u}^{k-1}$ and λ^{k-1}.
(3) Solve for λ^k from (19) using $\boldsymbol{u}^k$.
(4) Repeat the steps 2–3 until convergence.

3.2 Solving (19)

To solve for $\lambda(\boldsymbol{x})$ from (19), we chose to work with the most straightforward case when this equation is satisfied, that is when $\lambda(\boldsymbol{x})$ is a delta function, which is nonzero only when the constraint function $\Phi(\boldsymbol{x})$ is non-zero. Of course, we require the gradient of λ over the space in our PDE (18), and the delta function is differentiable only when it is viewed as a generalized function. For simplifying the problem, we replace the delta function by a regularized delta function

$$\lambda(\boldsymbol{x}) = K\delta(\Phi(\boldsymbol{x}) \geq 0(\boldsymbol{x})) \approx K\xi(r), \quad (20)$$

where K is a strength factor, and the above yields a well-defined and differentiable Lagrange multiplier function $\lambda(\boldsymbol{x})$ as we require. The $\xi(\cdot)$ is a regularized distribution that is supported by a finite cross-sectional area in $\mathbb{R}^n$. It can also

be thought as $n - dim$ blobs around each point $\boldsymbol{x}$ in space, where $r = |\boldsymbol{x} - \boldsymbol{x}_0|$, is the distance from the center of the blob $\boldsymbol{x}_0$. The distribution function $\xi(\boldsymbol{x}) = \frac{\pi}{\sigma^2}g(\frac{r}{\sigma})$ is a regularization of the delta function, normalized so that its integral over the space is equal to unity. Here, σ is the radius of the blob, which is a measure of the extent of the spread of the blob, and g is a dimensionless distribution that vanishes at ∞. Note that in the limit as $\sigma \rightarrow 0$, ξ reduces to the delta function.

A choice for the g function is given by $g(w) = \frac{1}{\pi^2}e^{-w^2}$. For $n = 2$, for instance, the 2D delta function is separable, and will be computed from $\delta(x, y) = \delta(x)\delta(y)$. In addition, we smooth the final $\lambda(\boldsymbol{x})$ function by a Gaussian filter to ensure that its gradient is regular.

4 Specifics of the Constrained PDE (18)

Generally speaking, the functional f in (18) consists of two types of terms:

$$f = f^i + f^r \quad (21)$$

where f^i is an image- and data-driven term, and f^r is a regularizing term on the unknown function, here $\boldsymbol{u}$.

In the next subsections, we explain the specifics of the three functionals: the regularizers f^r, inequality constraints Φ, and the image-dependent functionals f^i.

4.1 Regularizer

The simplest choice of a regularizer functional f^r is the Dirichlet integral:

$$f^r = \int_{\Omega} ||\text{Trace}(D\boldsymbol{u}D\boldsymbol{u}^T)||d\boldsymbol{x} \quad (22)$$

that yields a pure diffusion operator in the PDE, i.e., $\text{div}(D\boldsymbol{u})$, and hence assumes a smoothly varying vector field over the whole Ω domain. More sophisticated regularizing integrals that respect the discontinuity over the high image gradients are proposed such as the anisotropic diffusion term in [2]. Other forms of regularizers and more general matrix-valued functions can be found in [8, 12]. We will utilize the regularization operator:

$$\text{div}(D\boldsymbol{u}) \quad (23)$$

in our specific PDEs.

4.2 Image-Dependent Functionals

The data-driven term of the cost functional is chosen depending on the vision application.
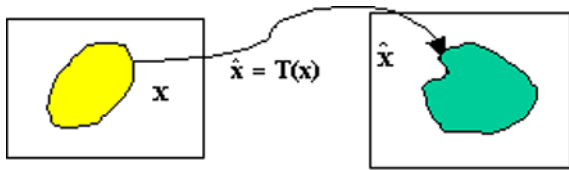
Fig. 2 Non-rigid mapping between two images defined through the coordinate transformation: $T(x) = x + u$

A joint non-rigid registration and segmentation approach For segmentation of a structure appearing in multiple domains, Unal et al. [36] presented a joint non-rigid registration and segmentation technique that utilized an infinite-dimensional transform $\hat{x} = T(x)$ where each point in domain Ω can move freely to a point in domain $\hat{\Omega}$ as depicted in Fig. 2.

We briefly summarize this technique as follows. Given two image volumes, $I : \Omega \in \mathbb{R}^n \rightarrow \mathbb{R}$ and $\hat{I} : \hat{\Omega} \in \mathbb{R}^n \rightarrow \mathbb{R}$, we denote the transformation that deforms one of the images to the other one by: $\hat{x} = T(x) = x + u(x)$, where $u(x)$ is the displacement vector field defined as $u : \Omega \rightarrow \mathbb{R}^n$ ($n = 2$ or 3). The goal is to find a surface $S \in \Omega$ that deforms on the first image I whereas a surface $\hat{S} \in \hat{\Omega}$ corresponding to the mapping $\hat{S} = T(S)$ deforms on the second image $\hat{I}$. Both surfaces move according to a generic image region-based energy functional defined over both image domains depending on region descriptors for the unknown foreground region, $f^{i,f}$, and the background region, $f^{i,b}$:

$$E(u, S) = \int_\Omega f^{i,f}(x)\chi^f(x)dx$$
$$+ \int_\Omega f^{i,b}(x)(1 - \chi^f(x))dx$$
$$+ \int_{\hat{\Omega}} \hat{f}^{i,f}(\hat{x})\chi^f(\hat{x})d\hat{x}$$
$$+ \int_{\hat{\Omega}} \hat{f}^{i,b}(\hat{x})(1 - \chi^f(\hat{x}))d\hat{x} \quad (24)$$

where χ^f denotes an indicator function for the foreground region over an image domain, $\hat{f}^{i,f}$ and $\hat{f}^{i,b}$ are the region descriptors for the foreground and the background in the transformed domain $\hat{\Omega}$. Note that in this case there is an additional unknown, the boundaries between the foreground and the background regions, i.e. the surface S for segmentation, and a proper regularizer on S is also introduced through the surface area integral $\int_S dA$ that induces a curvature term in the resulting segmentation PDE.

The solutions to the minimization problems are given by:

$$\tilde{S} = \arg\min_S E(S, u), \quad \text{and}$$
$$\tilde{u} = \arg\min_u E(S, u). \quad (25)$$

The surface evolution is given by:

$$\frac{\partial S}{\partial t} = f^i(x)N + \hat{f}^i(x + u(x))\hat{N} + \kappa N. \quad (26)$$

Note that $f^i = f^{i,f} - f^{i,b}$, and $\hat{f}^i = \hat{f}^{i,f} - \hat{f}^{i,b}$, N is the normal vector to the surface S, and $\hat{N}$ is the normal vector to the transformed surface $\hat{S}$, and κ is the curvature function for the surface S.

For registration evolution, the only part of the energy functional in (24) that is taken into account is:

$$E(u) = \int_\Omega \underbrace{\hat{f}^{i,f}(x + u(x))\chi^f(x + u(x))}_{F^f(x+u(x))} dx$$
$$+ \int_\Omega \underbrace{\hat{f}^{i,b}(x + u(x))(1 - \chi^f(x + u(x)))}_{F^b(x+u(x))} dx. \quad (27)$$

The gradient of E w.r.t. u is $\frac{\partial E}{\partial u} = \nabla_u F^f(u) + \nabla_u F^b(u)$, where ∇_u denotes the functional gradient w.r.t. u. We derive the PDE (over domain Ω) whose steady state solution gives the minimizer displacement field u which varies over space. The contributing term to our constrained PDE (18) from the image functional is then:

$$\frac{\partial u(x, t)}{\partial t} = \nabla_u \hat{f}^{i,f}(x + u(x))\chi^f(x + u(x))$$
$$+ \nabla_u \hat{f}^{i,b}(x + u(x))(1 - \chi^f(x + u(x)))$$
$$+ \hat{f}^i(x + u(x))\nabla_u(\chi^f(x + u(x))), \quad (28)$$

$$u(x, 0) = u_o(x).$$

For the third term above, the derivative of the indicator function χ with respect to u is intuitively a delta function over the boundaries between the foreground and the background region, and is defined in the sense of distributions. In practice regularized versions of a Heaviside function H and a delta function δ are used, particularly within a level set implementation $\phi : \Omega \rightarrow \mathbb{R}$ which represents S as its zero level set [7]:

$$\frac{\partial u(x, t)}{\partial t} = \nabla_u \hat{f}^{i,f}(x + u(x))H(\hat{\phi}(x + u(x)))$$
$$+ \nabla_u \hat{f}^{i,b}(x + u(x))(1 - H(\hat{\phi}(x + u(x))))$$
$$+ \hat{f}^i(x + u(x))\delta(\hat{\phi}(x + u(x))) \quad (29)$$
$$\times \nabla\hat{\phi}(x + u(x)),$$

$$u(x, 0) = u_o(x).$$

A special case for the image dependent functional f^i can be chosen as a simplified Mumford-Shah model [24], that is the piecewise constant model by Chan-Vese [7] that approximates the target regions in a given image I by the mean
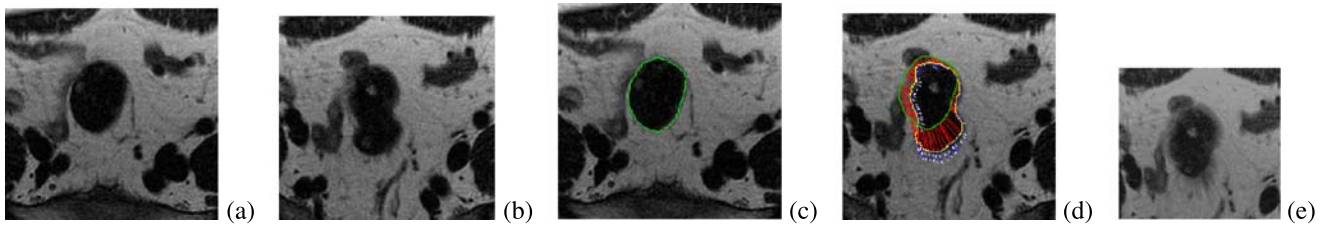
Fig. 3 (Color online) A 2D MR image pair at different slice levels (**a**, **b**). The structure's deformation is recovered by the (30), (26) depicted with the vector field whose direction goes from *red* to *blue* (**c**, **d**), i.e., *green* contour to *yellow* contour. The second image is deformed by the estimated vector field (**e**)

statistics. For instance, for a foreground region with a statistic m_f, and a background region with a statistic m_b, the specific form of f^i becomes

$$f^i(\boldsymbol{x}, \boldsymbol{u}) = (I(\boldsymbol{x} + \boldsymbol{u}) - m_f)^2 \chi^f(\boldsymbol{x})$$
$$+ (I(\boldsymbol{x} + \boldsymbol{u}) - m_b)^2 (1 - \chi^f)(\boldsymbol{x}).$$

With the piecewise (p-w) constant model for the target regions that are to be segmented and registered in images I and $\hat{I}$, the region-based term in the energy, and the gradient terms are given by:

$$\hat{f} = \hat{f}^{i,f} - \hat{f}^{i,b} = 2(\hat{m}_f - \hat{m}_b)$$
$$\times \left(\frac{\hat{m}_f + \hat{m}_b}{2} - \hat{I}(\boldsymbol{x} + \boldsymbol{u}(\boldsymbol{x})) \right),$$

$$\nabla_{\boldsymbol{u}} \hat{f}^{i,f} = 2(\hat{I}(\boldsymbol{x} + \boldsymbol{u}(\boldsymbol{x})) - \hat{m}_f) \nabla \hat{I}(\boldsymbol{x} + \boldsymbol{u}(\boldsymbol{x})),$$

$$\nabla_{\boldsymbol{u}} \hat{f}^{i,b} = 2(\hat{I}(\boldsymbol{x} + \boldsymbol{u}(\boldsymbol{x})) - \hat{m}_b) \nabla \hat{I}(\boldsymbol{x} + \boldsymbol{u}(\boldsymbol{x})),$$

where $\hat{m}_f$ and $\hat{m}_b$ are the mean of the image intensities inside and outside the surface mapped onto the second image volume domain respectively. These expressions can be inserted into (28) to obtain the PDE, which flows in the gradient descent direction, for evolution of non-rigid registration field for the p-w constant region model:

$$\frac{\partial \boldsymbol{u}(\boldsymbol{x},t)}{\partial t} = -(\hat{m}_f - \hat{m}_b) \left[\frac{(\hat{m}_f + \hat{m}_b)}{2} - \hat{I}(\boldsymbol{x} + \boldsymbol{u}(\boldsymbol{x})) \right]$$
$$\times \delta(\hat{\phi}(\boldsymbol{x} + \boldsymbol{u}(\boldsymbol{x}))) \nabla \hat{\phi}(\boldsymbol{x} + \boldsymbol{u}(\boldsymbol{x}))$$
$$- (\hat{I}(\boldsymbol{x} + \boldsymbol{u}(\boldsymbol{x})) - \hat{m}_f) \nabla \hat{I}(\boldsymbol{x} + \boldsymbol{u}(\boldsymbol{x}))$$
$$\times H(\hat{\phi}(x + \boldsymbol{u}(\boldsymbol{x}))) \qquad (30)$$
$$- (\hat{I}(\boldsymbol{x} + \boldsymbol{u}(\boldsymbol{x})) - \hat{m}_b) \nabla \hat{I}(\boldsymbol{x} + \boldsymbol{u}(\boldsymbol{x}))$$
$$\times (1 - H(\hat{\phi}(\boldsymbol{x} + \boldsymbol{u}(\boldsymbol{x}))))$$

$$\boldsymbol{u}(\boldsymbol{x}, 0) = \boldsymbol{u}_o(\boldsymbol{x}) = \boldsymbol{0},$$

where a zero vector field initialization is adequate in solving the PDE without any prior knowledge of the true vector field $\boldsymbol{u}$.

In Fig. 3, two different slices of an MR image sequence depict a dark structure in the middle, and which is jointly registered and segmented by the PDEs (30), (26), and (23). The result of deforming the second image region of interest (that is around and inside the contour) with the estimated vector field towards the first image particularly shows the success of the estimation.

In some segmentation applications, the basic approach of thresholding has proven to be useful. Instead of using means inside and outside the surface, one can convert such a basic "Chan-Vese" flow to a "thresholding" flow. This is also equivalent to region growing to separate the intensity inside the growing surface from the outside by the given threshold. For this purpose we use the following speed function:

$$\hat{f} = (\hat{m}_f - \hat{m}_b)(T - \hat{I}(\boldsymbol{x} + \boldsymbol{u}(\boldsymbol{x}))) \qquad (31)$$

where the $\frac{\hat{m}_f + \hat{m}_b}{2}$ quantity in "Chan-Vese" flow is replaced by an arbitrary threshold T. For this speed function we use the image terms on right hand side of the following PDE for updating the vector field:

$$\frac{\partial \boldsymbol{u}(\boldsymbol{x},t)}{\partial t} = -(\hat{m}_f - \hat{m}_b)(T - \hat{I}(\boldsymbol{x} + \boldsymbol{u}(\boldsymbol{x})))$$
$$\times \delta(\hat{\phi}(\boldsymbol{x} + \boldsymbol{u}(\boldsymbol{x}))) \nabla \hat{\phi}(\boldsymbol{x} + \boldsymbol{u}(\boldsymbol{x})), \qquad (32)$$
$$\boldsymbol{u}(\boldsymbol{x}, 0) = \boldsymbol{u}_o(\boldsymbol{x}) = \boldsymbol{0},$$

applied to the boundary term only.

For a tracking application, the image-based functional term can also be chosen as an image matching penalty $\int (I(\boldsymbol{x}) - \hat{I}(\boldsymbol{x} + \boldsymbol{u}(\boldsymbol{x})))^2 d\boldsymbol{x}$, as in the popular optical flow equation. Then the image matching term becomes:

$$\frac{\partial \boldsymbol{u}(\boldsymbol{x},t)}{\partial t} = -(I(\boldsymbol{x}) - \hat{I}(\boldsymbol{x} + \boldsymbol{u}(\boldsymbol{x}))) \, \nabla(\hat{I}(\boldsymbol{x} + \boldsymbol{u}(\boldsymbol{x}))). \quad (33)$$

One can note that although the flows are presented for between two image domains, this idea can be extended to multiple coordinate spaces to non-rigidly register a single common contour with multiple target objects.

4.3 Divergence Inequality Constraints

A natural constraint on the displacement vector field $\boldsymbol{u}$ is a constraint on the its divergence div $\boldsymbol{u}$. The divergence of a 2-dimensional vector field $\boldsymbol{u} = (u^x, u^y)$ is defined as the trace of its Jacobian matrix

$$D\boldsymbol{u} = \begin{bmatrix} \frac{\partial u^x}{\partial x} & \frac{\partial u^x}{\partial y} \\ \frac{\partial u^y}{\partial x} & \frac{\partial u^y}{\partial y} \end{bmatrix}. \tag{34}$$

Let us suppose we want to constrain the divergence of a vector field by a constant, say c, then the constraint function becomes

$$\Phi(x, \boldsymbol{u}, D\boldsymbol{u}) = \text{Trace}(D\boldsymbol{u}) - c \tag{35}$$

where c is a constant scalar function. To obtain the constrained PDE in this specific case, we write the differentials of Φ to find

$$\Phi_{D\boldsymbol{u}} = \frac{\partial}{\partial D\boldsymbol{u}}(\text{Trace}(D\boldsymbol{u}) - c) = \mathbf{Id} \tag{36}$$

where $\mathbf{Id}$ denotes the identity matrix. Therefore, for the goal of constraining divergence of the vector field from below, say by a given constant c_1, and from above, say by a given constant c_2 in a given variational vision problem, we set up two constraint functions:

$$\Phi^1(\boldsymbol{x}, D\boldsymbol{u}) = c_1 - \text{div } \boldsymbol{u}(\boldsymbol{x}) \leq \mathbf{0}, \tag{37}$$

$$\Phi^2(\boldsymbol{x}, D\boldsymbol{u}) = \text{div } \boldsymbol{u}(\boldsymbol{x}) - c_2 \leq \mathbf{0}. \tag{38}$$

Then we define two Lagrange multiplier functions, $\lambda^1(\boldsymbol{x})$ and $\lambda^2(\boldsymbol{x})$, which contribute to the specific form of our constrained PDE (18) as the operators

$$\Phi^1_{D\boldsymbol{u}}\nabla\lambda^1(\boldsymbol{x}) + \Phi^2_{D\boldsymbol{u}}\nabla\lambda^2(\boldsymbol{x}) = -\nabla\lambda^1(\boldsymbol{x}) + \nabla\lambda^2(\boldsymbol{x}). \tag{39}$$

Figure 4 depicts an application of the divergence constraints (37–38) on a vector field estimation. Here, as compared to joint registration and segmentation application, the idea is to use one contour and a vector field on the same image I. The vector field that defines the mapping between the inner boundary around the black circular region and

the outer boundary can be easily estimated using the PDE terms in (30) and regularizer term in (23). The resulting segmentation (contour) and the vector field are shown in (b). To demonstrate the effect of the inequality constraints on the divergence of the vector field, we apply the constraints $c_1 \leq \text{div}\boldsymbol{u} \leq c_2$, with $c_1 = 0.1$ and $c_2 = 0.3$. The initialized vector field that satisfies the constraint $\text{div}\boldsymbol{u} = c_1$ is shown in (c). Figure 4(d) shows the result of the evolution of the PDE (39) with the auxiliary equation (19) to solve for the Lagrange multiplier functions λ^1 and λ^2.

We will show applications of the divergence inequality constraints to a segmentation problem in Sect. 5.

4.4 Curl Inequality Constraints

A complementary idea to the divergence constraint is the usage of a curl constraint on a vector field. In fluid dynamics, curl of a vector field is defined as the vorticity. The intuition then in a tracking application is to put vorticity constraints on the vector field.

The curl constraint function can be written as

$$\Phi(x, \boldsymbol{u}, D\boldsymbol{u}) = \text{Trace}\, \boldsymbol{J}(D\boldsymbol{u}) - v \leq \mathbf{0} \tag{40}$$

where $\boldsymbol{J}$ denotes a 90 degree rotation on the Jacobian matrix, and v denotes a given vorticity of the vector field. Taking derivative of Φ w.r.t. $\boldsymbol{u}$ in this case yields:

$$\Phi_{D\boldsymbol{u}} = \frac{\partial}{\partial D\boldsymbol{u}}(\text{Trace}\, \boldsymbol{J}(D\boldsymbol{u}) - v) = \boldsymbol{J}. \tag{41}$$

Similar to the divergence constraints in the previous section, vorticity of a vector field can be limited from both below and above with two values of vorticity v_1 and v_2

$$\Phi^1(\boldsymbol{x}, D\boldsymbol{u}) = v_1 - \text{curl}\boldsymbol{u}(\boldsymbol{x}) \leq \mathbf{0}, \tag{42}$$

$$\Phi^2(\boldsymbol{x}, D\boldsymbol{u}) = \text{curl}\boldsymbol{u}(\boldsymbol{x}) - v_2 \leq \mathbf{0}. \tag{43}$$

Then we define two Lagrange multiplier functions, $\lambda^1(\boldsymbol{x})$ and $\lambda^2(\boldsymbol{x})$, which contribute to our constrained PDE (18) in
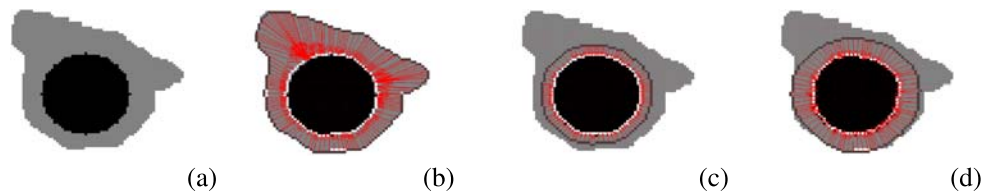

Fig. 4 The divergence inequality constraint on the vector field that maps the inner boundary towards the utter boundary demonstrated on the image in (**a**) (negative of the vector field is depicted). (**b**) Evolution without any constraint. (**c**) Initialized vector field with a divergence inequality constraint. (**d**) Resulting vector field with divergence constrained evolution
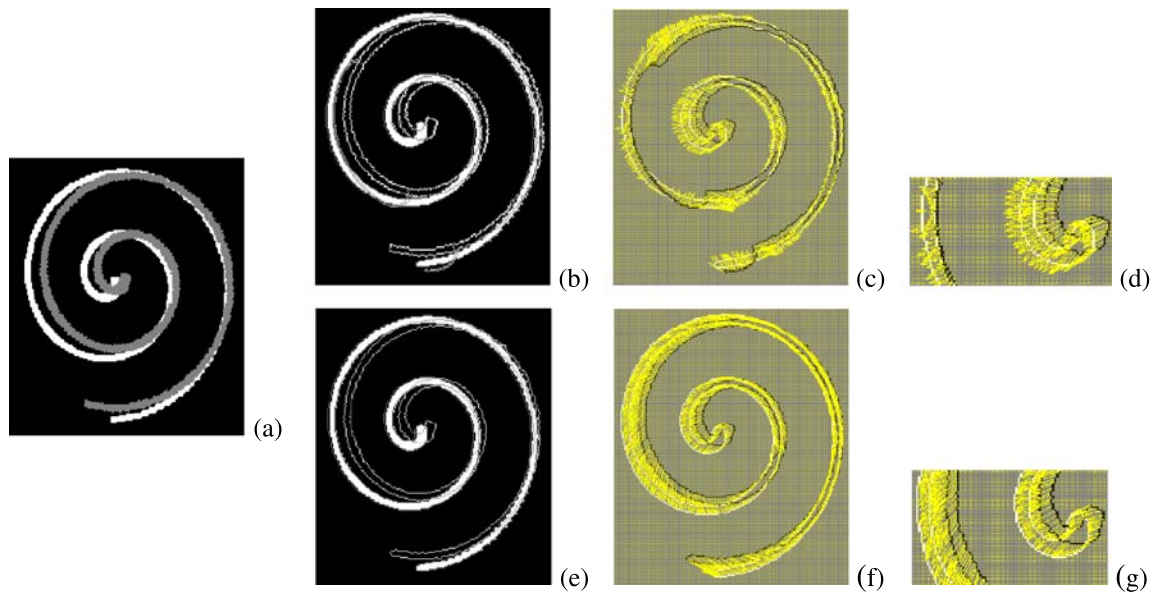
Fig. 5 Two synthetically generated spirals, where the white spiral is deformed by a vector field with only vorticity $(= 0.3)$ to form the gray spiral in (**a**). Without any vector field constraints, the estimated vector field through PDEs (30) and (23) produce incorrect results in (**c**) (zoomed section shown in (**d**) and (**b**) shows the two contours only). The estimated vector field is correct when the vorticity constraint terms (44) are added to the PDEs with $v_1 = 0.13$ and $v_2 = 0.33$, shown in (**f**) (zoomed section in (**g**)) and the two contours in (**e**)

the specific form of the operators

$$\Phi^1_{D\boldsymbol{u}} \nabla \lambda^1(\boldsymbol{x}) + \Phi^2_{D\boldsymbol{u}} \nabla \lambda^2(\boldsymbol{x})$$
$$= -\boldsymbol{J} \nabla \lambda^1(\boldsymbol{x}) + \boldsymbol{J} \nabla \lambda^2(\boldsymbol{x}). \tag{44}$$

Figure 5 shows two synthetically created spirals and estimation of the vector field mapping the gray spiral to the white spiral correctly estimated in presence of the constrained PDEs with the terms (44).

4.5 Translational Inequality Constraints

In case of translational constraints on a vector field, one intuitive idea is to constrain the amount of change on the first variation of the vector field, that is its Jacobian matrix. We limit the amount of change in the direction of the vector field by limiting the change in the norm of the Jacobian matrix, hence penalizing too much directional change. This can be done, for instance, by devising an inequality constraint involving the Frobenius norm of the Jacobian matrix of the vector field:

$$\Phi(x, \boldsymbol{u}, D\boldsymbol{u}) = ||(D\boldsymbol{u})||^2_F \leq \boldsymbol{\epsilon}, \tag{45}$$

where $||A||_F = \sqrt{\text{Trace}(A^T A)}$, and ϵ is a given small number that determines the amount of change allowed on the first variation of the vector field $\boldsymbol{u}$. This again leads to two constraint functions:

$$\Phi^1(\boldsymbol{x}, D\boldsymbol{u}) = \epsilon - \text{Trace}(D\boldsymbol{u}^T D\boldsymbol{u}) \leq \boldsymbol{0}, \tag{46}$$

$$\Phi^2(\boldsymbol{x}, D\boldsymbol{u}) = \text{Trace}(D\boldsymbol{u}^T D\boldsymbol{u}) - \epsilon \leq \boldsymbol{0}. \tag{47}$$

In this case, the differential of Φ is obtained using

$$\Phi_{D\boldsymbol{u}} = \frac{\partial}{\partial D\boldsymbol{u}} (\text{Trace}(D\boldsymbol{u}^T D\boldsymbol{u}) - \epsilon) = D\boldsymbol{u}^T, \tag{48}$$

and the two Lagrange multiplier functions, $\lambda^1(\boldsymbol{x})$ and $\lambda^2(\boldsymbol{x})$, contribute to the specific form of our constrained PDE (18) as the operators

$$\Phi^1_{D\boldsymbol{u}} \nabla \lambda^1(\boldsymbol{x}) + \Phi^2_{D\boldsymbol{u}} \nabla \lambda^2(\boldsymbol{x})$$
$$= -D\boldsymbol{u}^T \nabla \lambda^1(\boldsymbol{x}) + D\boldsymbol{u}^T \nabla \lambda^2(\boldsymbol{x}). \tag{49}$$

4.6 Magnitude of Vector Field Inequality Constraints

Another idea in constrained problems of vector fields is to restrict the amount of change on the magnitude of the vector field. This would be required if one wants to keep the vector field magnitude more or less within some bounds. As done in previous subsections, we write the corresponding inequality constraint involving the pointwise $\mathcal{L}_2$ norm squared of the vector field:

$$\Phi(x, \boldsymbol{u}, D\boldsymbol{u}) = ||\boldsymbol{u}||^2_2 \leq \boldsymbol{\epsilon}, \tag{50}$$

where $||\boldsymbol{u}||^2_2 = \boldsymbol{u}^T \boldsymbol{u}$, and ϵ is a given small number that determines the amount of change allowed on the norm of the vector field $\boldsymbol{u}$. In this case the two constraint functions:

$$\Phi^1(\boldsymbol{x}, \boldsymbol{u}) = \epsilon - \boldsymbol{u}^T \boldsymbol{u} \leq \boldsymbol{0}, \tag{51}$$
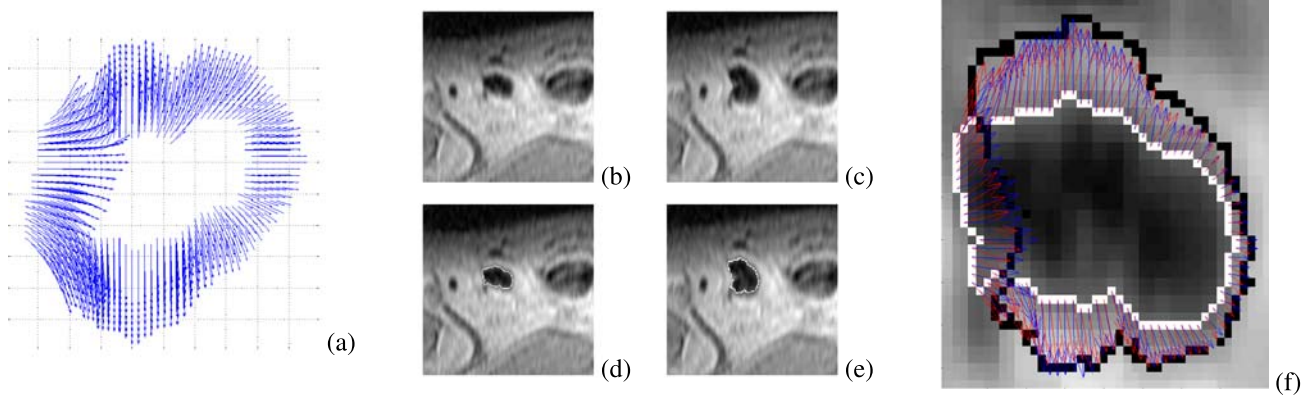
Fig. 6 (Color online) (**a**) Known spatially varying synthetic motion field. MR image segment including a lymph node without (**b**) and with the converged contour (**d**); Deformed image with the known vector field without (**c**) and with the converged contour (**e**). Zoomed section in (**f**) showing the ground truth (GT) vector field (*blue*) and the estimated vector field (*red*)

$$\Phi^2(\boldsymbol{x}, \boldsymbol{u}) = \boldsymbol{u}^T \boldsymbol{u} - \epsilon \leq 0 \tag{52}$$

with the differential of Φ simply:

$$\Phi_{\boldsymbol{u}} = \frac{\partial}{\partial \boldsymbol{u}}(\boldsymbol{u}^T \boldsymbol{u} - \epsilon) = 2\boldsymbol{u}^T, \tag{53}$$

lead to the constrained PDEs

$$\frac{\partial \boldsymbol{u}(\boldsymbol{x})}{\partial t} = \Phi_{\boldsymbol{u}}^1 \lambda^1(\boldsymbol{x}) - \Phi_{\boldsymbol{u}}^2 \lambda^2(\boldsymbol{x})$$
$$= 2\boldsymbol{u}^T(\boldsymbol{x})\lambda^1(\boldsymbol{x}) - 2\boldsymbol{u}^T(\boldsymbol{x})\lambda^2(\boldsymbol{x}). \tag{54}$$

5 Experiments and Conclusions

For the numerical implementation of the contours, we utilized a level set representation [26, 33] for convenience. Due to a narrowband level set implementation, we will most effectively be solving for $\boldsymbol{u}(\boldsymbol{x})$ on a band around the surface. We present the application of the technique in both 2D and 3D spaces. For the volumetric images, such as in brain MRI and the abdomen CT examples, the implementation is in 3D space, and the resulting surfaces along with the 3D vector field and contours from each slice are shown in 2D. For the remaining 2D images presented below, the method is applied in 2D space.

5.1 Experiments in Coupled Non-Rigid Registration and Segmentation Without Constraints

We simulated a non-rigid deformation by creating a completely arbitrary spatially varying motion field using nonlinear functions and a modified normal vector field, as shown in Fig. 6(a) around the structure of interest only. We deformed with this known motion field the real input image data in (b) showing an image segment with a lymph node in an MR image sequence, and this resulted in the image depicted in (c).

Table 1 The average and standard deviation of the angle between GT and the estimated vector field, and the mean-squared error

Distortion Measure	Error
Average Angle ($\boldsymbol{u}_{GT} - \boldsymbol{u}_{EST}$)	0.07π (13°)
Standard Deviation Angle ($\boldsymbol{u}_{GT} - \boldsymbol{u}_{EST}$)	0.04π (7°)
MSE ($\boldsymbol{u}_{GT} - \boldsymbol{u}_{EST}$)	1.65

The comparison is done using the angle between the ground truth deformation field and the estimated deformation field obtained with (30). The results displayed in the Table 1 show an average angle difference of 13° with a standard deviation of 7°. The mean squared error between these two vector fields is found to be 1.65.

The computational complexity of the algorithm in 3D is as follows. Since we are computing the PDEs in (26) and (30) over a narrow-band around the zero level set of the surface in $\mathbb{R}^3$ (usually radius of the band is chosen as 5), the general complexity is $O(N^2)$. For the computation of the means inside and outside the image volume for Eq. (26), the complexity is $O(N^2)$ except at initialization it is $O(N^3)$ (going through all the image volume). For the computation of the means inside and outside the second image volume for (30) or (32), the second band (surface) is initialized after the first band (surface) is updated every time, therefore with the current implementation the complexity is $O(N^3)$, but it is possible to compute it at $O(N^2)$.

When the target structures in the two image domains do not overlap, either automated pre-processing using Dicom header information for physical coordinates to initialize the vector field, or first jointly executing a rigid registration flow, or an interactive registration to roughly align the two volumes are possible solutions.

Next we show an example for segmentation and registration of corpus callosum from MR brain image volumes. In

neurology and neurocognitive science, the size and shape of the corpus callosum in human brain has shown to be correlated to different factors of humans and the human brain [22]. Therefore, inter-patient studies of corpus callosum(cc) characteristics is an important problem and requires estimation of transformations among cc shapes in a population of patients. We jointly segment and estimate a vector field between two different patients cc shapes as demonstrated in Fig. 7 which shows evolution of the surface and the final estimated deformation field between the cc of the two patients. For inter-patient studies, such a vector field may be used to obtain a measure of shape and size differences between surfaces of cc's of two patients and thus proves to be useful.

Figure 8 shows the T1 MRI volumes of the same brain example from two patients (only one slice from the MRI volume is shown). In this experiment, the "Chan-Vese" flow easily leaks to surrounding regions during the evolutions, therefore does not perform successfully. Instead the "thresholding" flow in (32) along with the corresponding surface evolution flow (26) are used with a threshold of $T = 60$
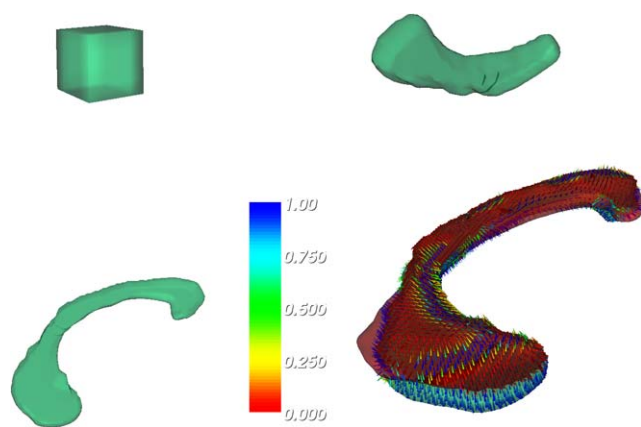
whereas the image volumes has the intensity range (0,255). Therefore, with a simple modification to the simplest piecewise constant model and with a quickly obtained prior information from the intensity in the initialized seed surface, we could obtain a reasonable segmentation and registration result as the initial and final contours can be observed in Fig. 8.

In the example in Fig. 9, two CT image volumes of the same patient taken at different time points are segmented and registered using (26)–(30) for delineating the bladder volume at different time periods.

For a multi-modality application, for instance, a post-contrast T2-weighted MR image and a T2* echo weighted MR image, are shown in Fig. 10, where the regions and boundaries of a target structure, a malignant node, exhibit different characteristics. We utilize the piecewise constant model with a non-unit variance term $f^i = \frac{(\hat{I}(x+u) - \hat{m}_f)^2}{\hat{\sigma}_f^2} \chi^f + \frac{(\hat{I}(x+u) - \hat{m}_b)^2}{\hat{\sigma}_b^2}(1 - \chi^f)$ to obtain the
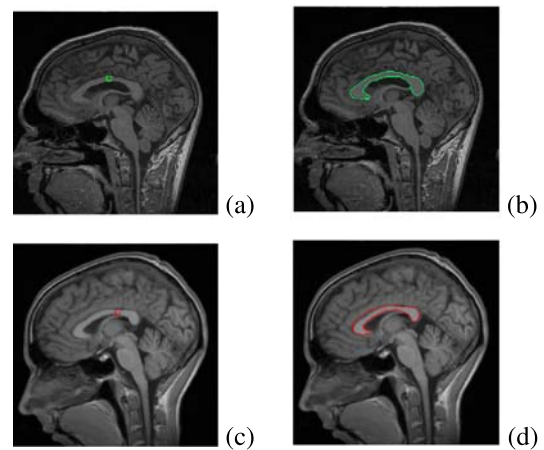

(a) (b) (c) (d)

Fig. 8 Sagittal T1 MRI volumes from different patients (a slice shown in **a**–**b**) with in-plane resolution 0.44 mm and another patient (a slice shown in **c**–**d**) with in-plane resolution 0.97 mm: here note the mis-alignment between the corpus callosum of the two patients; after the non-rigid registration and segmentation has been applied, the resulting corpus callosum surfaces are shown in (**b**) and (**d**)

Fig. 7 (Color online) Evolution of the surface over the corpus callosum (*top row* and *bottom left*) along with the estimated vector field from the first patient's corpus callosum (shown in *green*) towards the second one (shown in *red*)

Fig. 9 (Color online) CT image slices of a patient at different times shown on rows 1 and 2. A seed is given in the bladder (*left*) and the resulting segmentation and registration on the bladder (*middle*). The surface shows the deformation of the first surface towards the second (*right*)
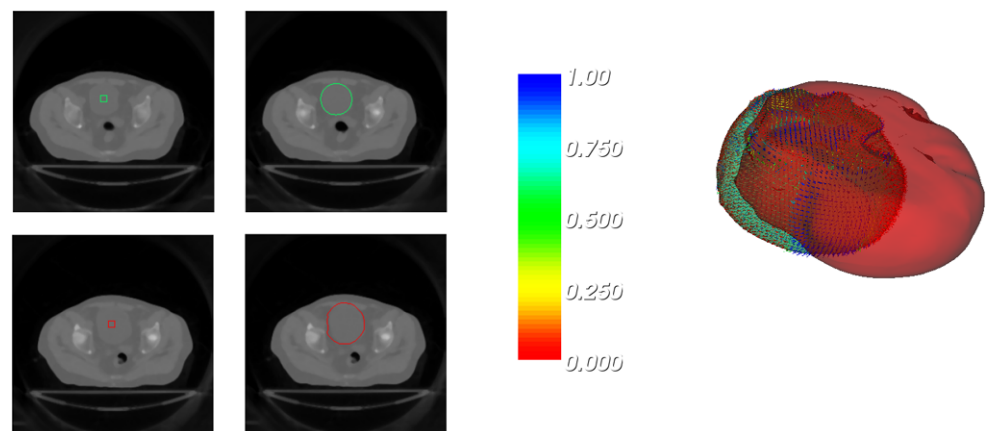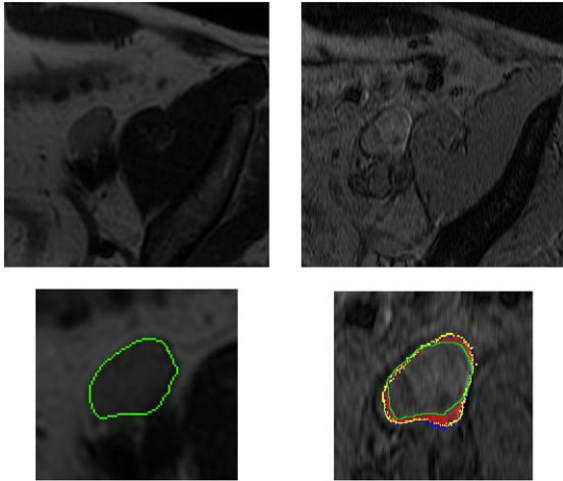
Fig. 10 (Color online) Using a non-unit variance flow, the node on the T2 image (*green*) is morphed onto the node on the T2* echo image (*yellow*) on the *right*

Fig. 11 Myocardium image shown at end-systole phase in (**a**). When there are no constraints on the vector field estimation, the result of segmentation of the myocardium through the estimated vector field fails because it converges to the trivial solution of zero vector field (**b**) (zoomed in (**c**)). The vector field estimation is successful in case the inequality constraints in (39) are activated initially in (**d**) and finally in (**e**) (zoomed in (**f**))

deformation field between the nodes in T2 and T2* echo images. However, in multi-modality applications like this one, it is expected that utilizing more features to explain and account for a variety of region and boundary characteristics is desirable. One possible extension of our work includes incorporation of boundary-based information in deriving the non-rigid registration PDE or using piecewise-smooth region models.

5.2 Experiments in Constrained Problems

The divergence inequality constraints are applied to segmentation of myocardium in MR images. Figure 11 shows an end-systole phase of the heart beat in (a). Without the divergence constraint terms (39) in our vector field evolution PDE, the image terms can not guarantee a vector field evolution that would keep the solution away from the trivial one,
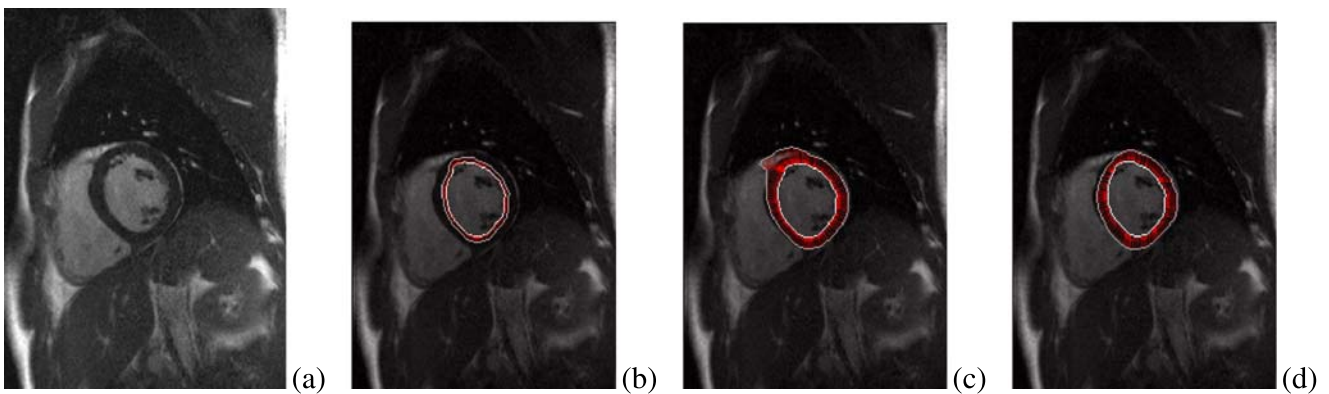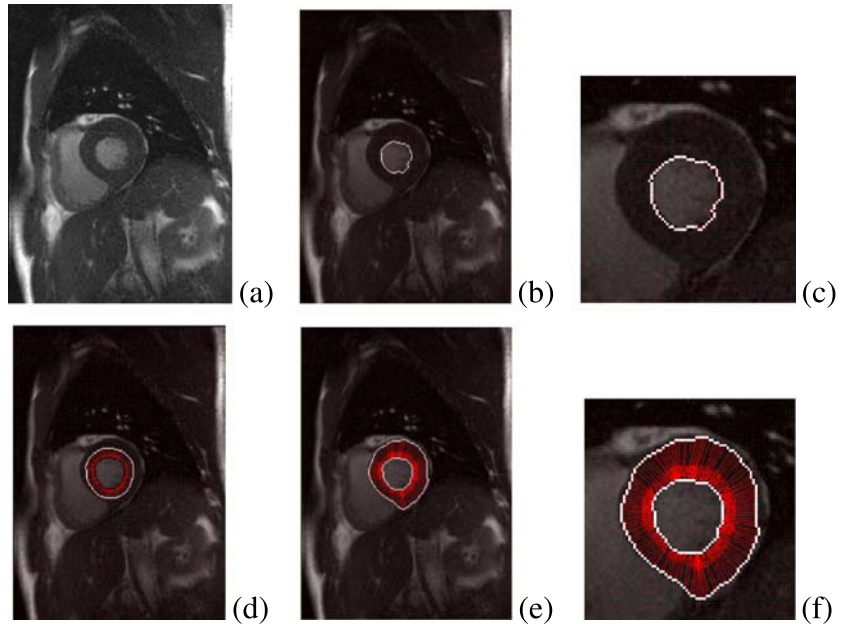

Fig. 12 Myocardium image shown at end-diastole phase in (**a**). The initial vector field shown in (**b**) is evolved without any divergence inequality constraints in (**c**), and fails. A better estimation is obtained

when the divergence inequality constraints (39) are activated, and results in a better segmentation of the myocardium through the estimated vector field in (**d**)
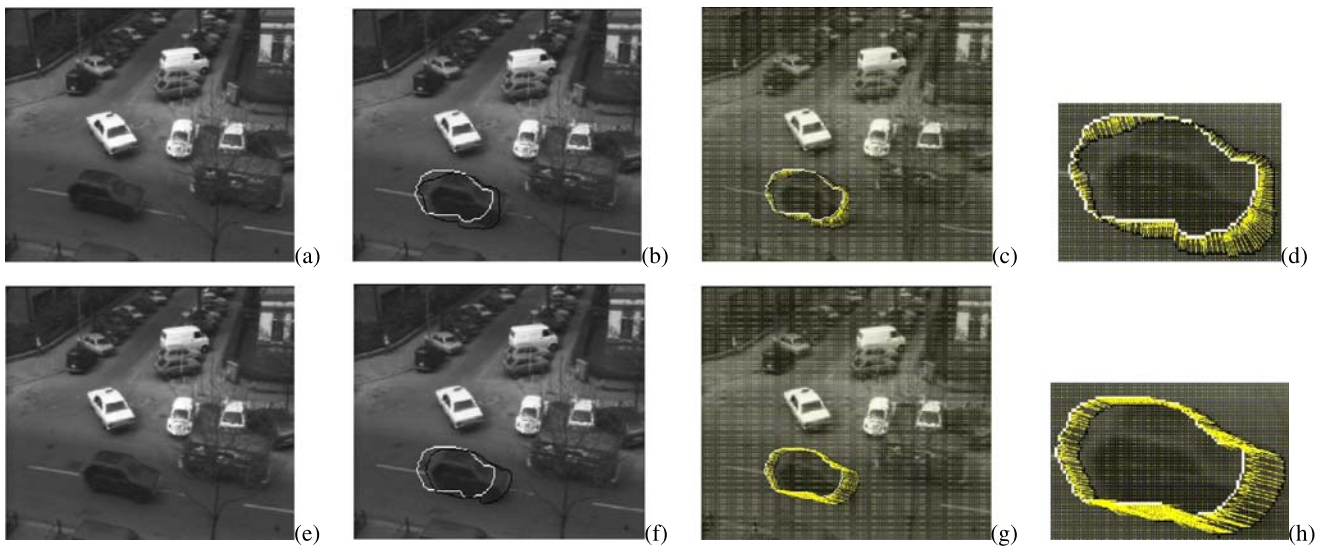
Fig. 13 Two frames in (**a**) and (**e**) from the taxi image sequence (downloaded from KOGS/IAKS Universitat Karlsruhe) demonstrate the constraint on the norm of the Jacobian of the vector field plus the constraint on the vector field norm itself. (**b**) and (**c**) show the resulting segmentations and vector field estimates when the vector field is evolved without any inequality constraints, hence fails (zoomed section in (**d**)). The vector field estimation is successful in case the inequality constraints (54) are activated as depicted in (**f**) and (**g**) (zoomed section in (**h**))
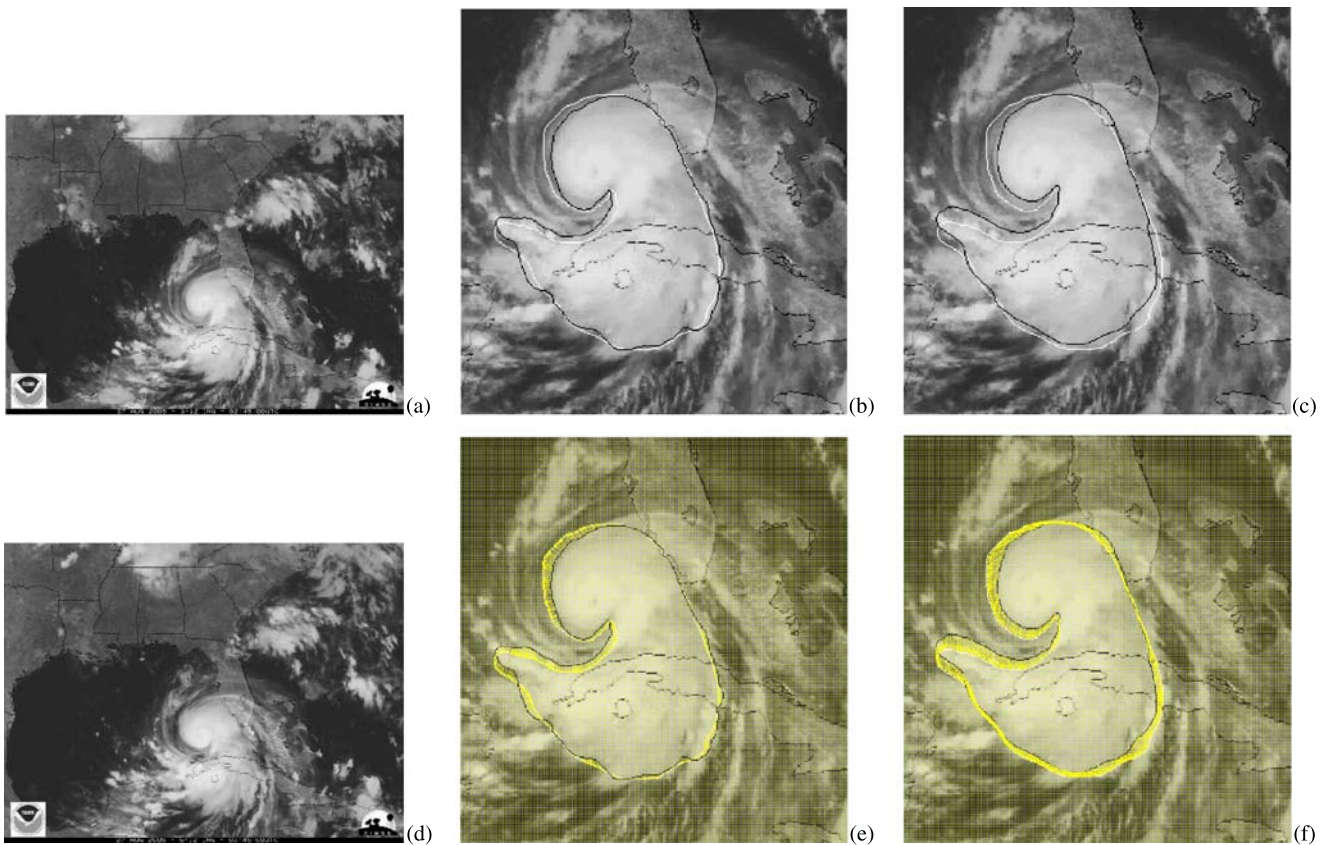

Fig. 14 Two frames in (**a**) and (**d**) from the hurricane Katrina image sequence demonstrate the constraint on the curl of the vector field. (**b**) and (**e**) show the resulting segmentations (*white contour* represents the segmentation on the first frame, and *black contour* on the second frame, both are shown as superimposed on the second image frame) and vector field estimates when the vector field is evolved without any inequality constraints, which evolves towards the initial contour without strong features from the image. The vector field estimation is more likely to be considered as successful in case the inequality constraints of the PDE (44) are activated (**c**) and (**f**), although there is no ground truth knowledge for this example

that is a zero vector field as shown in (b) with which the energy of the contour is minimized. Instead, the PDE with divergence constraints leads to the correct solution as shown initially in (d) and result in (e) (zoomed in (f)). In this experiment, the divergence constraint from below ($\text{div} \boldsymbol{u} \geq c$) helps the flow correctly propagate to the solution.

In the next experiment, for the myocardium image at end-diastole in Fig. 12(a), the divergence constraint from above ($\text{div} \boldsymbol{u} \leq c$) steps up to drive the vector field evolution to a better solution in (d) in contrast to the unconstrained PDE result in (c), where both evolutions were initialized with the vector field in (b).

We show the effect of translation and norm constraints on the vector fields in Fig. 13 for the taxi sequence. The optical flow is estimated between the two frames of the taxi sequence shown in (a) and (e). When the vector field is estimated without any inequality constraints, the resulting registration was not successful as depicted in (b)-segmentations, i.e. the contours, and (c)–(d)-the vector field estimate. The vector field estimation was successful in case the inequality constraints (54) are activated as shown in (f)–(h).

We show the effect of curl constraint on the vector fields in Fig. 14 for the hurricane Katrina sequence (downloaded from National Oceanic and Atmospheric Administration www.noaa.gov). The hurricane is winding outwards from the center in this sequence. The constrained solution is better than the unconstrained solution, as expected. However, the data terms, which we use, do not exactly model this difficult image scenario. If in addition to the constrained PDE terms, one can incorporate good image features that model the image better than piecewise constant mean image, to the data term of the PDEs, the results can be expected to improve.

5.3 Conclusions

In this paper, we described utilization of local inequality constraints via Kuhn-Tucker theorem in interesting variational problems of computer vision, which require estimation of vector fields that model deformations between objects in multiple images. We showed applications in coupled registration and segmentation problems in medical imaging and tracking problems in vision. We believe that our work will stir up new questions and lead to developments in the utilization of inequality constrained variational problems in the computer vision community.

References

1. Abraham, R., Marsden, J., Ratiu, T.: Manifolds, Tensor Analysis and Applications. Springer, New York (1988)
2. Alvarez, L., Weickert, J., Sánchez, J.: Reliable estimation of dense optical flow fields with large displacements. Int. J. Comput. Vis. **39**(1), 41–56 (2000)
3. Amit, Y.: A nonlinear variational problem for image matching. SIAM J. Sci. Comput. **15**(1), 207–224 (1994)
4. Aubert, G., Deriche, R., Konrprobst, P.: Computing optical flow via variational techniques. SIAM J. Appl. Math. **60**(1), 156–182 (1999)
5. Bertalmio, M., Caselles, V., Rouge, B., Sole, A.: Tv based image restoration with local constraints. J. Sci. Comput. **19**(1–3), 95–122 (2003)
6. Bliss, G.A.: Calculus of Variations. Carus Mathematical Monographs. MAA, Chicago (1925)
7. Chan, T., Vese, L.: An active contour model without edges. In: Int. Conf. Scale-Space Theories in Computer Vision, pp. 141–151 (1999)
8. Chefd'hotel, C., Hermosillo, G., Faugeras, O.: A variational approach to multi-modal image matching. In: VLSM Workshop-ICCV, pp. 21–28 (2001)
9. Chefd'Hotel, C., Tschumperle, D., Deriche, R., Faugeras, O.: Regularizing flows for constrained matrix-valued images. J. Math. Imaging Vis. **20**, 147–162 (2004)
10. Chen, Y., Tagare, H., Thiruvenkadam, S., Huang, F., Wilson, D., Gopinath, K., Briggs, R., Geiser, E.: Using prior shapes in geometric active contours in a variational framework. Int. J. Comput. Vis. **50**(3), 315–328 (2002)
11. Cherkaev, A., Cherkaev, E.: Calculus of variations and applications. Lecture Notes, University of Utah, Salt Lake City, UT (2003)
12. Christensen, G.E., Rabbitt, R.D., Miller, M.I.: Deformable templates using large deformation kinematics. IEEE Trans. Image Process. **5**(10), 1435–1447 (1996)
13. Cremers, D., Soatto, S.: Variational space-time motion segmentation. In: Proc. Int. Conf. on Computer Vision, pp. 886–982 (2003)
14. Desbrun, M., Hirani, A., Marsden, J.: Discrete exterior calculus for variational problems in computer vision and graphics. In: CDC Conference (2003)
15. Dydenko, I., Friboulet, D., Magnin, I.: A variational framework for affine registration and segmentation with shape prior: application in echocardiographic imaging. In: VLSM-ICCV, pp. 201–208 (2003)
16. Gelfand, I.M., Fomin, S.V.: Calculus of Variations. Dover, New York (1963)
17. Gregory, J., Lin, C.: Constrained Optimization in the Calculus of Variations and Optimal Control Theory. Chapman and Hall, New York (1992)
18. Horn, B.K.P., Schunck, B.G.: Determining optical flow. Artif. Intell. **17**, 185–203 (1981)
19. Keeling, S., Ring, W.: Medical image registration and interpolation by optical flow with maximal rigidity. J. Math. Imaging Vis. **23**(1), 47–65 (2005)
20. Lantéri, H., Roche, M., Aime, C.: Penalized maximum likelihood image restoration with positivity constraints: multiplicative algorithms. Inverse Probl. **18**, 1397–1419 (2002)
21. Luenberger, D.G.: Optimization by Vector Space Methods. Wiley, New York (1969)
22. Lundervold, A., Taxt, T., Duta, N., Jain, A.: Model-guided segmentation of corpus callosum in mr images. In: Proc. IEEE Conf. on Computer Vision and Pattern Recognition, pp. 1231–1236 (1999)
23. Modersitzki, J.: Numerical Methods for Image Registration. Oxford University Press, London (2004)
24. Mumford, D., Shah, J.: Boundary detection by minimizing functionals. In: Proc. IEEE Conf. on Computer Vision and Pattern Recognition, San Fransisco, pp. 22–26 (1985)
25. Nagy, J., Strakos, Z.: Enforcing nonnegativity in image reconstruction algorithms. In: D.C.W. et al., (eds.) Mathematical Modeling, Estimation, and Imaging, vol. 4121, pp. 182–190 (2000)

26. Osher, S., Sethian, J.: Fronts propagating with curvature dependent speed: Algorithms based on the Hamilton-Jacobi formulation. J. Comput. Phys. **49**, 12–49 (1988)

27. Paragios, N., Deriche, R.: Geodesic active regions for motion estimation and tracking. In: Proc. Int. Conf. on Computer Vision, pp. 224–240 (1999)

28. Paragios, N., Rousson, M., Ramesh, M.: Knowledge-based registration and segmentation of the left ventricle: A level set approach. In: IEEE Workshop on App. Comp. Vision, pp. 37–42 (2002)

29. Paragios, N., Rousson, M., Ramesh, V.: Non-rigid registration using distance functions. Comput. Vis. Image Underst. **89**, 142–165 (2003)

30. Polthier, K., Preuss, E.: Variational approach to vector field decomposition. In: Eurographics Workshop on Visualization, Springer (2000)

31. Ray, K., Majumder, D.: A critical appreciation on algebraic image restoration. IEEE Trans. Syst. Man Cybern. **18**(3), 477–481 (1988)

32. Richard, F., Cohen, L.: A new image registration technique with free boundary constraints: Application to mammography. In: Proc. European Conf. Computer Vision, pp. 531–545 (2002)

33. Sethian, J.: Level Set Methods and Fast Marching Methods. Cambridge University Press, Cambridge (1999)

34. Simard, P., Mailloux, G.: A projection operator for the restoration of divergence-free vector fields. IEEE Trans. Pattern Anal. Mach. Intell. **10**(2), 248–256 (1988)

35. Tong, Y., Lombeyda, S., Hirani, A., Desbrun, M.: Discrete multiscale vector field decomposition. In: Proc. ACM SIGGRAPH (2003)

36. Unal, G., Slabaugh, G.: Coupled pdes for non-rigid registration and segmentation. In: Proc. IEEE Conf. on Computer Vision and Pattern Recognition, vol. 1, pp. 168–175 (2005)

37. Vemuri, B., Chen, Y.: Joint image registration and segmentation. In: Osher, S., Paragios, N. (eds.) Geometric Level Set Methods in Imaging, Vision and Graphics, pp. 251–269. Springer, New York (2003)

38. Wang, F., Vemuri, B.: Simultaneous registration and segmentation of anatomical structures from brain mri. In: MICCAI, LNCS, vol. 3749, pp. 17–25, October 2005

39. Wong, A., Liu, H., Shi, P.: Segmentation of myocardium using velocity field constrained front propagation. In: IEEE Workshop Applications of Computer Vision, p. 84 (2002)

40. Wyatt, P., Noble, J.: Map mrf joint segmentation & registration. In: MICCAI, pp. 580–587 (2002)

41. Yezzi, A., Zollei, L., Kapur, T.: A variational framework for joint segmentation and registration. In: CVPR-MMBIA, pp. 44–49 (2001)

42. Yezzi, A., Zollei, L., Kapur, T.: A variational framework for integrating segmentation and registration through active contours. Med. Image Anal. **7**(2), 171–185 (2003)

43. Zhang, T., Freedman, D.: Tracking objects using density matching and shape priors. In: Proc. Int. Conf. on Computer Vision, pp. 1056–1062 (2003)

Gozde Unal received the Ph.D. degree in electrical engineering from North Carolina State University, Raleigh, in August 2002, and later she was as a postdoctoral fellow at the Georgia Institute of Technology and visited HP Labs, Palo Alto, California, as a postdoctoral researcher during the summer of 2003. From Fall 2003 to 2007, she worked as a research scientist at Siemens Corporate Research, Princeton, New Jersey. She joined the faculty of Sabanci University, Istanbul, Turkey in Fall 2007, where she is currently an assistant professor. Her research interests include variational techniques with connection to information theory and probability theory, applications to various computer vision, and image processing problems such as stereoscopic camera calibration, 2D/3D image segmentation and registration, filtering and enhancement, and stochastic particle systems. Her current research is focused on medical image analysis, segmentation, registration, and shape analysis techniques with applications to clinically relevant problems in MR, CT, US, and intravascular images. She is a Senior Member of the IEEE, and Associate Editor for IEEE Transactions on Information Technology on Biomedicine.

Greg Slabaugh is a Research Scientist at Siemens Corporate Research, located in Princeton, NJ. He earned an M.S. and a Ph.D. in Electrical Engineering at the Georgia Institute of Technology under the supervision of Dr. Ronald W. Schafer, and a B.S. in Engineering Physics from the University of Michigan. He is currently an Associate Editor of IEEE Signal Processing Magazine, and co-organized the International Workshop on Computer Vision for Intravascular Imaging held in conjunction with MICCAI2006. Greg Slabaugh's main research interests are in computer vision, image processing, and computer graphics. More specifically, he is interested in medical image processing, 3D reconstruction from multiple images, new view synthesis, image and surface registration, tracking, segmentation, geometric modeling, adaptive filtering, PDEs, radial basis functions, deformable surfaces, and level set methods.